ANNALS OF GEOPHYSICS, 68, 6, G691, 2025; doi:10.4401/ag-9393
OPEN ACCESS

InSAR time-series results of the 2025 Santorini unrest, using Sentinel-1A data

Bekir Poyraz[*,1], Hüseyin Duman[2], Yavuz Gül[3], Fatih Poyraz[2], Kemal Özgür Hastaoğlu[2]

(1) Department of Physics, Faculty of Science, Sivas Cumhuriyet University, Sivas, 58140, Türkiye.
(2) Department of Geomatics Engineering, Faculty of Engineering, Sivas Cumhuriyet University, Sivas, 58140, Türkiye.
(3) Civil Engineering, Faculty of Engineering, Sivas Cumhuriyet University, Sivas, 58140, Türkiye.

Article history: received may 30, 2025; accepted November 26, 2025

Abstract

Santorini Island is of volcanic origin and has historically faced repeated volcanic and seismic activity. In early 2025, increased volcanism and intensified earthquake activity, similar to 2011-2012, caused residents' concern. This study aims to characterize ground deformation on Santorini Island during its volcanic unrest in 2025 using InSAR observations. For this purpose, 74 synthetic aperture radar (SAR) images of Sentinel-1A satellites in descending and ascending orbits were acquired from early January 2024 to late March 2025. Line-Of-Sight (LOS) velocity values of the descending and ascending orbits were decomposed to determine the east-west and vertical displacement velocities. According to the results obtained, uplifts up to +60 mm/year velocity values were detected in the central parts of the island called Caldera, and subsidence up to −30 mm/year velocity values were detected in the outer regions. In addition, eastward horizontal movements reaching velocities of +60 mm/year and westward horizontal movements reaching velocities of −50 mm/year were also detected throughout the island.

In the second stage of the study, a total of 4 points were selected on the islands of Thira, Thirasia, Nea Kameni, and Palea Kameni, considering the Kameni and Kolumbo fault zones. For these points on the island of Santorini, the displacements occurring over 15 months were analysed by time series analysis, and the temporal behaviour of the deformation (increasing/decreasing trend) was monitored. The analysed data indicate that the ongoing horizontal and vertical movements on the island could be caused by volcanic rather than seismic effects, which is consistent with previous studies. This situation shows that volcanic risk assessments in the region should be monitored for the upcoming processes.

Keywords: Santorini; InSAR; LOS; SBAS; Time Series

1. Introduction

Santorini Volcano has experienced a total of twelve Plinian (Plinian-type) eruptions in the last 200 to 300 thousand years, at least four of which led to caldera collapse (Pyle, 1997; Druitt et al., 2019; Antoniou et al., 2020). Plinian eruptions are an extremely powerful and explosive type of volcanic eruption. The term is named in honour of the Roman writer and naturalist Pliny the Younger, who described in detail the eruption of Mount Vesuvius in 79 AD (Tekin, 2016). The island of Santorini serves as a unique natural laboratory for the study of arc-arc volcanism.

The quiescent periods between Plinian eruptions are characterized by the formation of intracaldera structures and low-intensity strombolian (moderately explosive) activity. These large-scale eruptions are triggered by high-flow magma injections from deeper levels into magma chambers 4-8 km deep, starting centuries before the event (Druitt et al., 2019).

Santorini is one of the most spectacular caldera volcanoes in the world. The caldera depression was formed after a major eruption in which the volcanic dome collapsed as a result of the rapid discharge of the magma chamber (Nomikou et al., 2016; Kennedy, 2024). The Minoan town of Akrotiri has been the focus of considerable scientific and academic interest due to the large Bronze Age eruption that buried it (Druitt et al., 1999). Santorini is an active volcano belonging to the modern Aegean Volcanic Arc. The last major eruption, also known as the Minoan Eruption, occurred approximately 1627-1600 BC (Friedrich et al., 2006; Browning et al., 2015). Tons of ash and volcanic material buried the prehistoric city of Akrotiri. Rapidly spreading, superheated volcanic flows caused a tsunami, estimated to have reached a height of 30 m, which struck the coast of Crete and caused the decline of the Minoan civilisation (Druitt et al., 1999). Due to the enormous size of the eruption, some scientists claim that the eruption not only affected the Cyclades and the Aegean but also caused a worldwide climate change. Since then, the Santorini volcano has erupted several more times, continuously changing the morphology of the island (Pyle, 1997). The destruction of the central part of the island led to the formation of a caldera, resulting in the formation of the present-day islands of Thera, Therasia, and Aspronisi, arranged in a ring around a flooded caldera (Karátson et al., 2018). In 1950, the last lava emission and volcanic plume formation took place on Santorini and Nea Kameni, the newest landmass in Europe (Antoniou et al., 2020).

It is suggested that magma emplacement in Santorini occurred predominantly along the Kameni and Kolumbo fault zones (Mountrakis et al., 1996; Druitt et al., 1999) and the Christiana-Santorini-Kolumbo rift zone (Nomikou et al., 2016; Hooft et al., 2017; Heath et al., 2019). During the 2011-2012 unrest period, magma accumulation beneath the Kameni fault zone made the presence of a seismogenic crustal fault more evident (Newman et al., 2012; Feuillet, 2013). During this process, although the fault did not directly facilitate magma movement, some sections of the fault showed seismic movement due to crustal stress transfer partly due to the inflating magma chamber (Parks et al., 2012; Lagios et al., 2013; Papadimitriou et al., 2015). However, these movements did not cause rupture of the crustal magma chamber or the formation of a dyke (Browning et al., 2015). This suggests that changes in the local stress field can occur without dyke injection. The relationship between changes in the local stress field and magma emplacement in Santorini is still poorly understood. In particular, how dyke and fault interactions can leave traces in the geological record and how to evaluate them in terms of future dike propagation predictions requires further research (Drymoni et al., 2022).

The Santorini volcanic complex consists of four islands. Thirasia and Thira are well-known tourist destinations and form the edge of the caldera. The centres of Palea Kameni and Nea Kameni were built in the caldera. The Santorini Caldera has been the source of numerous eruptions and tsunamis in the past, with the last seismic sequence ending in 1950 (Druitt et al., 1999). Since then, the Santorini volcano has been in a ‘quiet’ phase with insignificant deformations (Stiros et al., 2010; Papageorgiou et al., 2011). Seismic activity was limited to a location 10 km northeast of Thera (Dimitriadis et al., 2009). However, this phase was interrupted in early 2011 (Papoutsis et al., 2013). In January 2011, the Santorini volcano entered a period of unrest, i.e., the ground surface began to swell, and the magnitude and frequency of earthquakes increased. This period lasted until April 2012, when signs of unrest ceased (Browning et al., 2015; Newman et al., 2012).

During 2011-2012, significant ground uplift occurred, reaching up to 14 cm over Nea Kameni, emphasised the seismo-volcanic unrest (Foumelis et al., 2013). Prolonged periods of quiescence interrupted by short periods of non-eruptive activity are similarly observed in other caldera volcanic systems (Taal, Philippines; Rabaul, Papua New Guinea; and other similar calderas) (Del Gaudio et al., 2010; Aiuppa et al., 2013; Wicks et al., 2006). A new episode of unrest, similar to that of 2011-2012, began to manifest at the beginning of 2025. Thousands of large and small earthquakes occurred in the region between January 2024 and March 2025, the largest of which was MW 5.2. The number of events with a magnitude of MW 3.0 or greater is presented in Table 1 (http://www.geophysics.geol.uoa.gr/stations/maps/recent.html, last access: April 18, 2025). Earthquakes with a magnitude of MW 4.0 or greater are concentrated in the north-eastern part of the study area (Fig. 1).

Recent advances in geodetic imaging techniques and the systematic availability of SAR data are expected to play an important role in re-evaluating the mechanisms of the deformation fields of Santorini Volcano before and after periods of unrest. In this study, the displacement time series are analysed and interpreted in terms of the last unrest.

Table 1. Number of earthquake events occurring in the Sea of Islands, Santorini island, and its surroundings in January 2024-March 2025 (http://www.geophysics.geol.uoa.gr/stations/maps/recent.html, last access: April 18, 2025).

Date	Earthquakes (Mw)			
	>3.0	>3.5	>4.0	>5.0
20240101-20240131	2			
20240201-20240229				
20240301-20240331				
20240401-20240430	1			
20240501-20240531				
20240601-20240630				
20240701-20240731	2			
20240801-20240831	1			
20240901-20240930	5	1		
20241001-20241031				
20241101-20241130	2			
20241201-20241231	3			
20250101-20250131	2	2		
20250201-20250228	1137	560	193	7
20250301-20250331	48	14	4	
Total	1207	577	197	7

Santorini (36° 24.264′N, 25° 23.865′E) is the southernmost volcanic centre of the Aegean island arc (Fig. 2). It is located on approximately 25 km of continental crust within a 40 km-wide NE-SW rift zone consisting of normal and right-lateral strike-slip faults (Durit, 2014). The regional fault systems are the NE-SW-striking Kameni and Kolumbo Fault Zones (Papageorgiou et al., 2019). With dimensions of approximately 11 × 8 km, it hosts the world's largest water-filled caldera. Palea and Nea Kameni are active volcanic centres. Other islands of Santorini are Thira, Thirasia, and Aspronisi. To the south-west are the Christiana volcanic islands, and to the north-east is the Kolumbo submarine volcano (Antoniou et al., 2020).

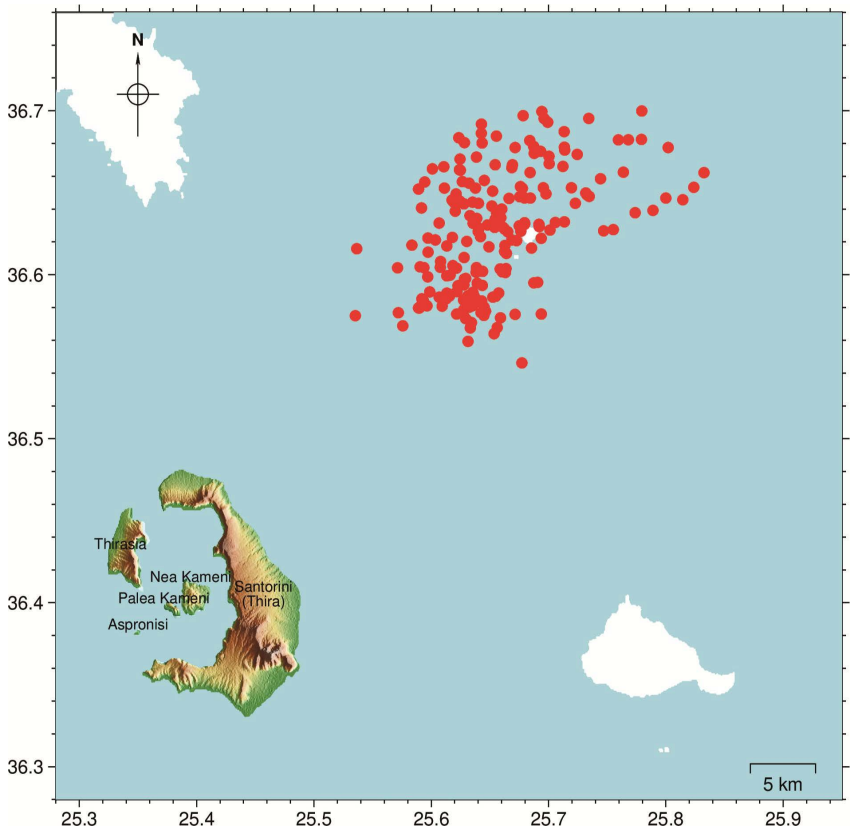

Figure 1. Seismic activity of magnitude Mw 4.0 and above in the Archipelago Sea, Santorini Island, and surrounding areas between January 2024 and March 2025 (red dots indicate earthquake locations).

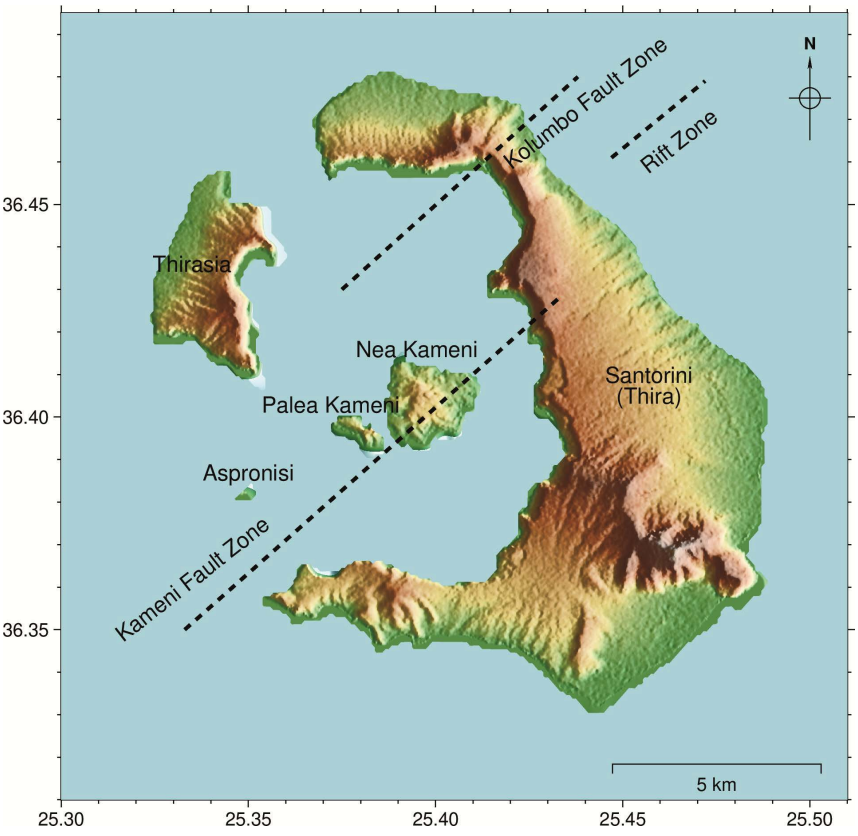

Figure 2. Santorini volcanic centre of the Aegean island arc. The world's largest water-filled caldera.

2. Material and methodology

2.1 Geodetic data

The geodetic data used in this study consist of Synthetic Aperture Radar (SAR) images acquired by the Sentinel-1A satellite in Interferometric Wide Swath (IW) mode, with a spatial resolution of 5 × 20 meters. A total of 37 ascending-track images (orbit number 21), acquired between 12 January 2024 and 31 March 2025, and 37 descending-track images (orbit number 109), acquired between 6 January 2024 and 25 March 2025, were processed.

Interferograms were generated using the open-source GMTSAR software, based on the Generic Mapping Tools (GMT) (Sandwell et al., 2011; Sandwell et al., 2016), and the Small BAseline Subset (SBAS) method. Interferogram pairs of ascending and descending orbits (69 for ascending and 67 for descending) are shown in Fig. 3, with a maximum temporal baseline of 30 days and a maximum spatial baseline of 400 meters. GMTSAR follows standard processing steps to generate interferometric products, including image coregistration using a 30-meter resolution Digital Elevation Model (SRTM1) and removal of the topographic phase component. The GMTSAR

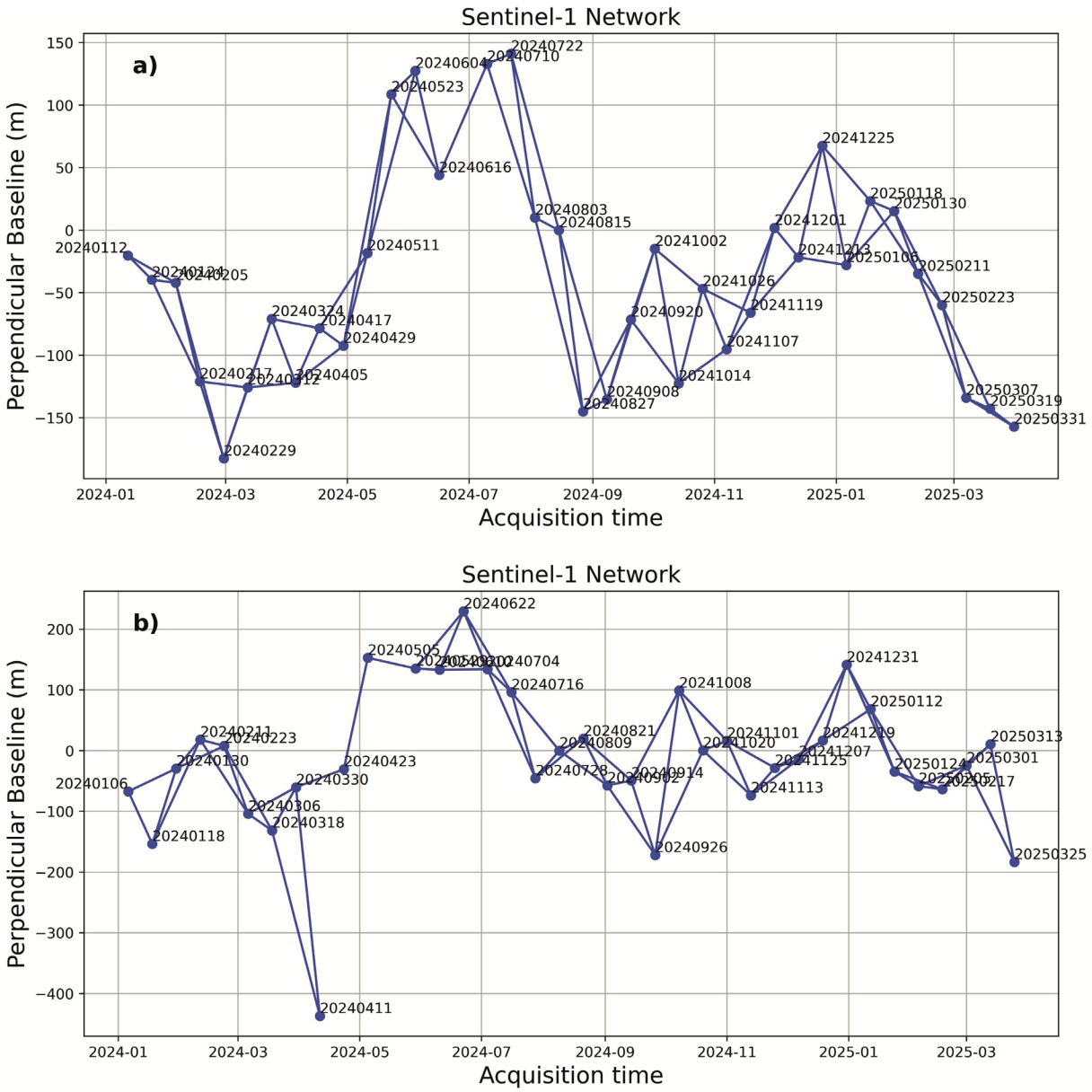

Figure 3. Spatial and temporal distribution of the Sentinel-1A images relative to SBAS (Blue lines indicate interferogram pairs). a) Ascending orbit (track 21; 69 pairs). b) Descending orbit (track 109; 67 pairs).

outputs were then processed with the Stanford Method for Persistent Scatters software (StaMPS) (Hooper et al., 2018), which was employed to estimate phase noise values for each pixel and to identify Distributed Scatter (DS) points. Following phase correction, phase unwrapping was performed using the Statistical-Cost, Network-Flow Algorithm for Phase Unwrapping (SNAPHU) (Chen and Zebker, 2001). Orbital errors were subsequently corrected using precise orbit information provided by ESA, while residual topographic errors were removed with the SRTM1. Atmospheric noise was estimated and mitigated through temporal and spatial filtering within the StaMPS framework, which distinguishes atmospheric artefacts from tectonic deformation by exploiting their different spatio-temporal characteristics (Hooper et al., 2007). After applying these corrections and filters, mean line-of-sight (LOS) velocities were derived (Fig. 4).

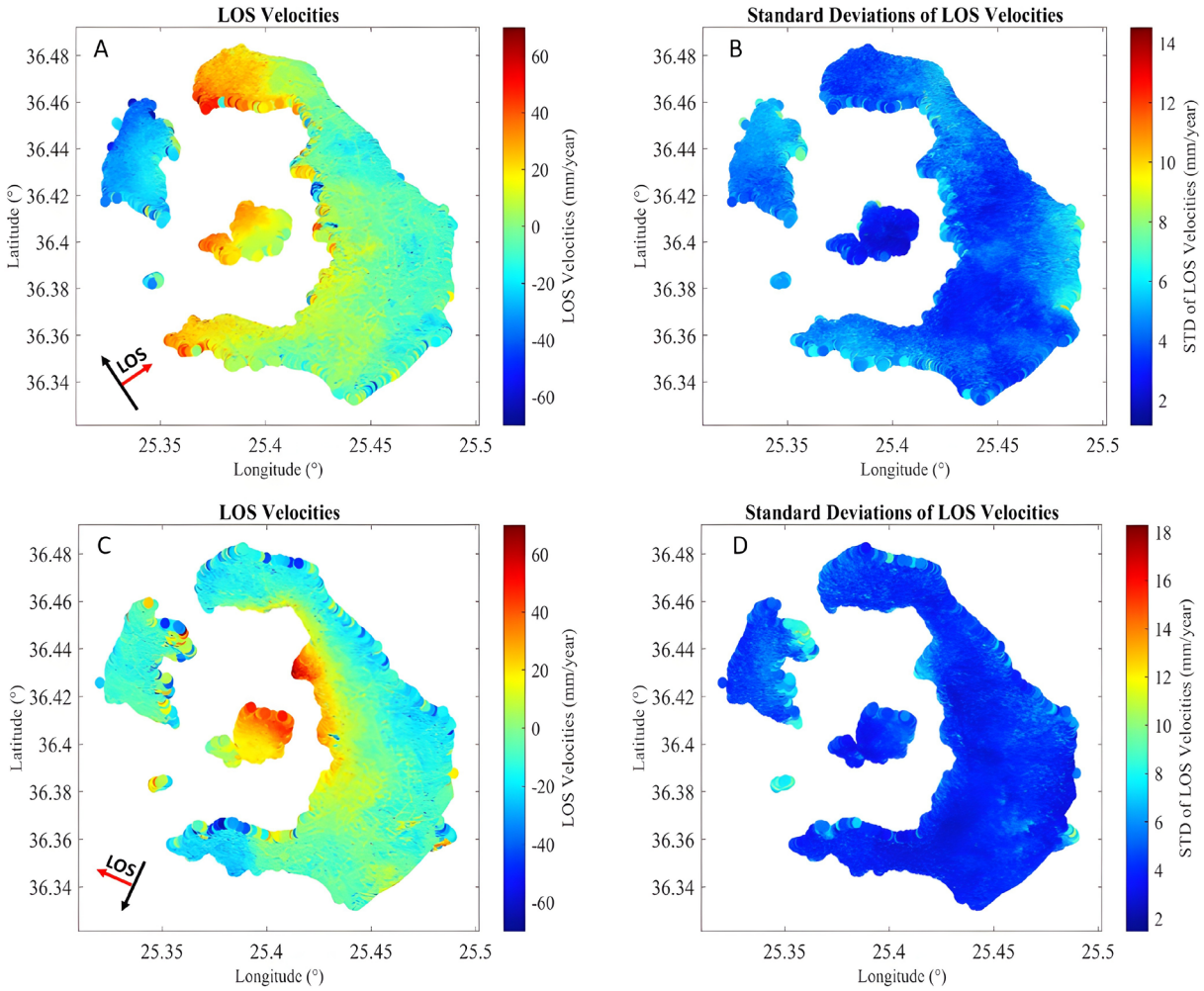

Figure 4. Line-of-sight (LOS) velocity and standard deviation maps (A-B: ascending orbit; C-D: descending orbit).

Using the equations given below, the velocities in the LOS direction were converted into horizontal and vertical components using the MineSAR software developed by the researchers who are among the authors of this study (Gül et al., 2025).

Although satellite radar data are measured in the one-dimensional line-of-sight (LOS) direction, ground surface deformation is typically represented by three components: east, north, and vertical. Equation 1 expresses the surface velocity vector (V_{LOS}) in the satellite line-of-sight direction. V_{LOS}, s, and V represent the LOS velocity, the satellite unit vector, and the three-dimensional surface velocity vector, respectively (Gül and Poyraz, 2024). In Eq. (2), the heading angle (α_h) and the incidence angle (δ) are applied for ascending and descending satellite passes (Arikan et al., 2010; Hastaoğlu, 2016; Fuhrmann and Garthwaite, 2019). In Eq. (3), the LOS velocity components of descending and ascending satellites are transformed into eastward and vertical velocity components (Hanssen,

2001). The northward component is neglected due to the Sentinel-1 satellite orbit configuration (Gül and Poyraz, 2024).

$$V_{LOS} = s^T \cdot V \tag{1}$$

$$s = (-\cos(\alpha_h)\sin(\delta) \quad \sin(\alpha_h)\sin(\delta) \quad \cos(\delta))^T \tag{2}$$

$$\begin{pmatrix} -\cos(\alpha_{ASC})\sin(\delta_{ASC}) & \cos(\delta_{ASC}) \\ -\cos(\alpha_{DSC})\sin(\delta_{DSC}) & \cos(\delta_{DSC}) \end{pmatrix} \begin{pmatrix} V_{EW} \\ V_{UP} \end{pmatrix} = \begin{pmatrix} V_{LOS,ASC} \\ V_{LOS,DSC} \end{pmatrix} \tag{3}$$

In Eq. (3), the heading angles for descending and ascending orbits are shown as α_{ASC} and α_{DSC}, and the incidence angles are shown as δ_{ASC} and δ_{DSC}. V_{UP} shows the vertical direction velocity, V_{EW} shows the easting direction velocity, $V_{LOS,ASC}$ and $V_{LOS,DSC}$ show the descending and ascending orbital velocities in the LOS direction (Gül and Poyraz, 2024). The obtained vertical and horizontal deformation velocity maps are given in Fig. 5.

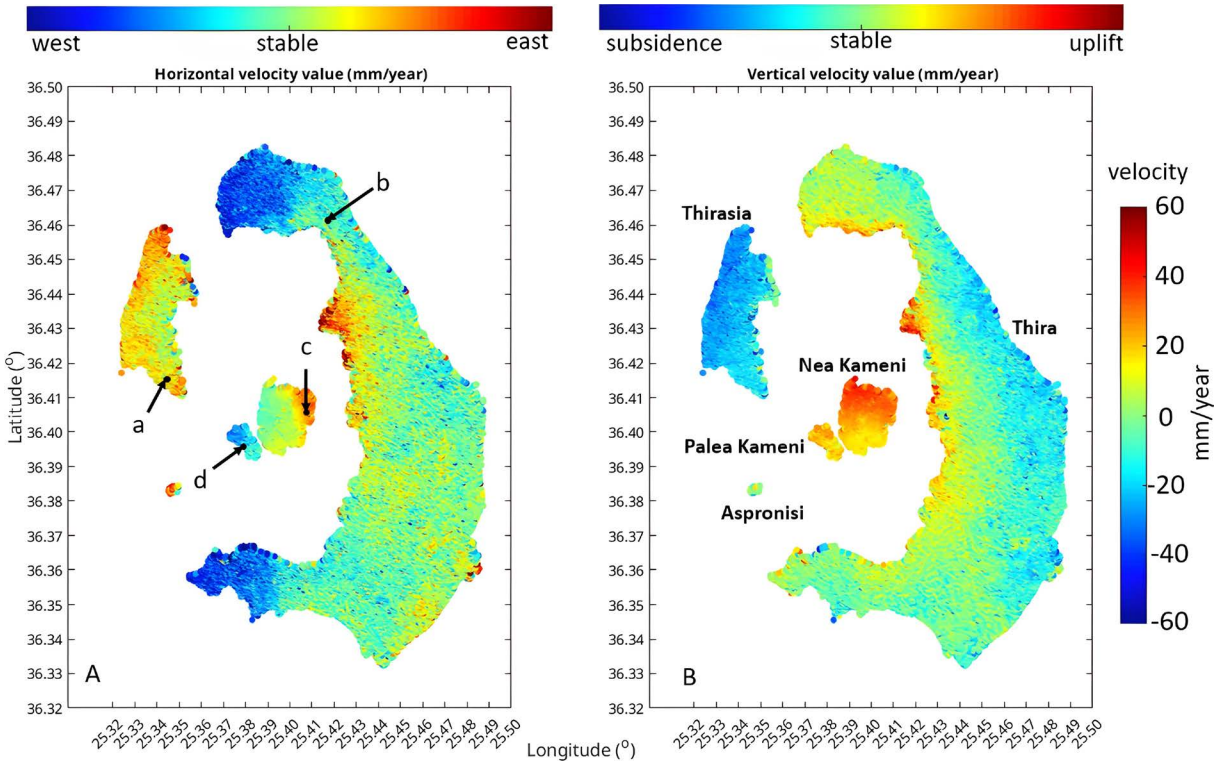

Figure 5. Deformation velocity maps of Santorini Island for the period 12 January 2024-31 March 2025 (A: Horizontal deformation velocities; B: Vertical deformation velocities).

In the second part of the study, a total of 4 points (a, b, c, and d points) were selected on the islands of Thira, Thirasia, Nea Kameni, and Palea Kameni (Fig. 5A), taking into account the Kameni and Kolumbo fault zones on the island of Santorini, where possible movements are most expected. Fig. 6 shows the 15-month displacement time series at selected points on the island of Santorini obtained using MineSAR software. MineSAR computes the median displacement value (blue dots) of the DS points (pink dots) located within a 30-meter-radius circle centred on each selected point. This approach reduces noise from individual DS points and allows the dominant deformation trends to be more clearly identified. The time series includes both horizontal (east-west) and vertical (uplift-subsidence) components, enabling detailed monitoring of deformation changes before and after this period, particularly in light of the earthquake swarm in early February 2025.

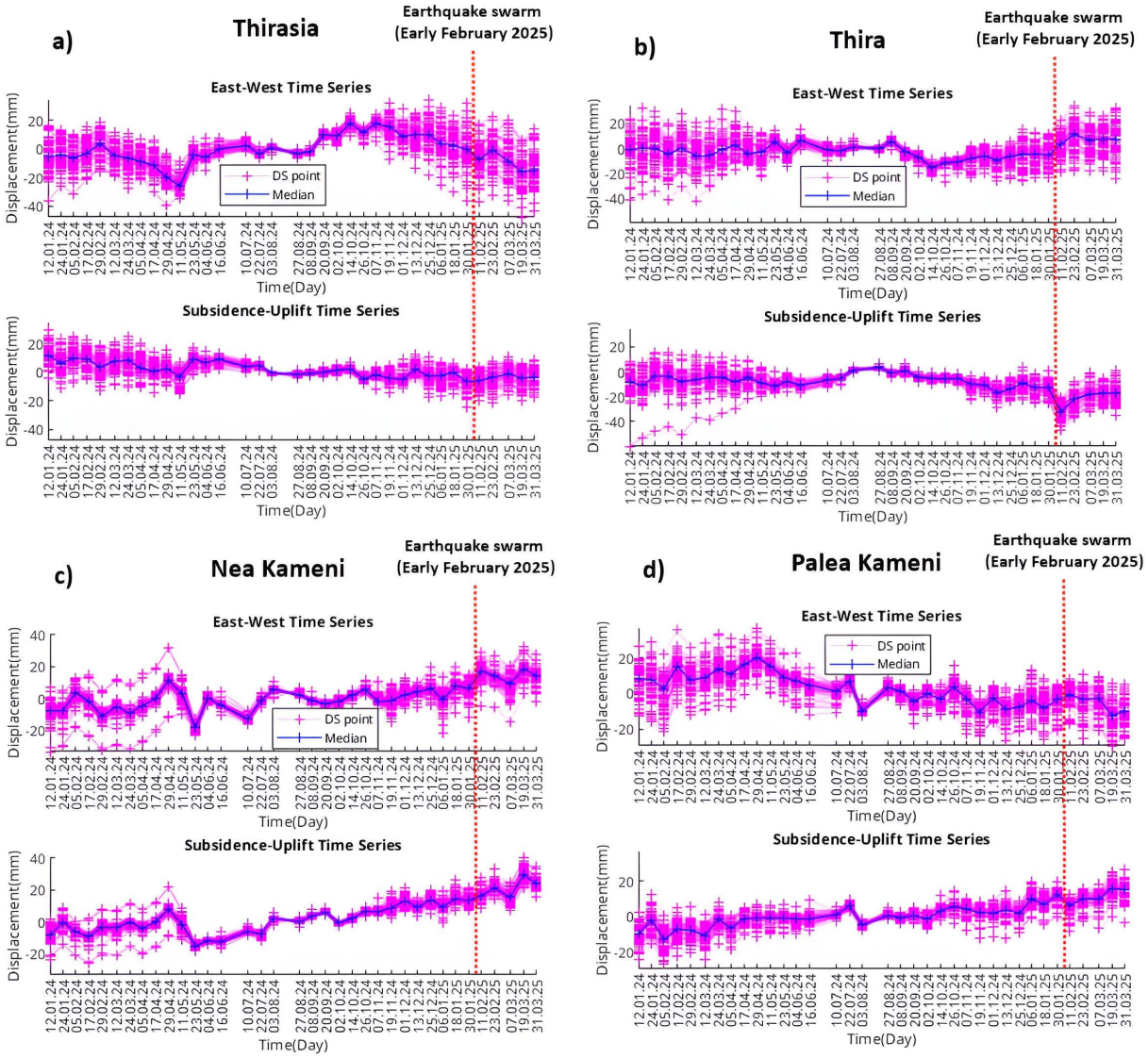

Figure 6. Time series graphs of displacements for points determined on the island of Santorini, see Fig. 5A

3. Results

In this study, InSAR analyses were applied to Santorini Island for the period January 2024-March 2025 to reveal the distribution of horizontal and vertical deformations associated with the new signs of unrest. Taking the peak earthquake activity of early February 2025 as a temporal reference, the deformation behaviour before and after this period was examined in detail.

In this context, firstly, the procedures detailed in Section 2 were carried out for the 15-month satellite SAR images obtained. The results obtained allow us to make the following assessments:

- As a result of examining the horizontal velocities obtained by decomposing the LOS velocities, Fig. 5A shows easterly deformation rates of +60 mm/yr and above were determined in the eastern part of Nea Kameni Island and in the western parts of Thira and Thirasia Islands. Furthermore, westerly deformation rates of −50 mm/yr and above were observed in the western part of Thira Island.
- When vertical velocities were examined, Fig. 5B shows uplifts of up to +60 mm per year were detected on the islands of Palea Kameni and Nea Kameni within the caldera and on the west coast of Thira, and subsidences of up to −30 mm per year were detected on the island of Thirasia and on the east coast of Thira.

In the second part of the study, considering the Kameni and Kolumbo fault zones on the island of Santorini, a total of 4 points (a, b, c, and d points) were selected on the islands of Thira, Thirasia, Nea Kameni, and Palea Kameni. The 15-month time series of deformations, before and after February 2025, when earthquakes on the island and in its surroundings were particularly intense, was examined in terms of increasing/decreasing trends, and the following observations were made.

- Point a (36° 25.132′N, 25° 20.724′E, Thirasia Island, near the Kolumbo Fault Zone): The horizontal movements do not show a periodic increasing and decreasing trend, varying between approximately −30 mm (west) and +20 mm (east) (Fig. 6a). These movements observed before the February 2025 earthquake swarm continued similarly in March 2025, despite the decrease in earthquake frequency and magnitude. This indicates that horizontal movements are not directly related to the swarm. The vertical movements vary between approximately +15 mm (uplift) and −5 mm (subsidence), both before and after the February 2025 earthquake swarm, without any obvious increasing or decreasing trend.
- Point b (36° 28.020′N, 25° 24.936′E, Thira Island, near the Kolumbo Fault Zone): Similar to point a, no clear increasing or decreasing trend is observed in the horizontal and vertical deformations. Horizontal movements vary between approximately −10 mm (west) and +10 mm (east), while vertical movements vary between approximately +5 mm (uplift) and −10 mm (subsidence) (Fig. 6b). These patterns remain consistent before and after the February 2025 earthquake swarm.
- Point c (36° 24.600′N, 25° 24.456′E, Nea Kameni Island, near the Kameni Fault Zone): Horizontal movements exhibit periodic increasing/decreasing trends (approximately −20 mm (west) to +15 mm (east) before October 2024), but they continued with an increasing trend starting from September 2024, including the period after the February 2025 earthquake swarm (+20 mm east). In vertical movements, there is a displacement in the form of a total uplift of approximately 60 mm, from −20 mm to +40 mm, with a clear increasing trend starting from May 2024 (Fig. 6c).
- Point d (36° 23.730′N, 25° 23.028′E, Palea Kameni Island, near the Kameni Fault Zone): Horizontal movements have exhibited an increasing trend in the west direction since April 2024, continuing after the February 2025 earthquake swarm (+20 mm to −20 mm, a total displacement of 40 mm). Vertical displacements, in the form of uplift (-10 mm to +20 mm), amount to a total of 30 mm since February 2024, and still show a tendency to increase (Fig. 6d).

4. Discussion

When the horizontal and vertical deformations observed on Santorini Island are considered as a whole, it becomes evident that the island has entered a new phase of unrest similar to the 2011-2012 period (Briole et al., 2025; Papazachos et al., 2025). Although the deformation in the region, especially in the form of uplift, existed before the earthquakes, it continues despite the significant decrease in the magnitude and number of earthquakes. These uplifts, which are concentrated in the Caldera region where points c and d are located, are interpreted as the result of magma chamber inflation. The fact that uplift deformation persisted even after the decline in seismicity indicates that crustal stress transfer within the magma chamber continues, suggesting that new seismic events could be triggered in the future.

The scientific meaning of these findings is that the deformation observed on Santorini is not merely a short-term response to past seismicity, but rather reflects the active state of the magmatic system beneath the caldera. This highlights the critical importance of continuous geodetic monitoring (e.g., InSAR and GNSS), as detecting stress accumulation may provide early warning of possible volcanic or seismic hazards. These results are consistent with previous studies (Browning et al., 2015; Newman et al., 2012; Foumelis et al., 2013; Briole et al., 2025; Papazachos et al., 2025), but also extend them by emphasizing that the current unrest is likely driven by magma-induced stress, which requires careful long-term observation.

5. Conclusions and reccomendations

This study aims to present the InSAR processing results for Santorini Island for the period January 2024-March 2025, focusing on the characterization of horizontal and vertical deformation patterns associated with the new

signs of unrest. After the seismic activity that increased in the region in February 2025, horizontal and vertical deformation analyses were performed on the island, which has attracted attention again, using satellite-derived SAR images covering 15 months. As a result of the observations, significant horizontal and vertical ground movements were detected, especially on the islands of Nea Kameni and Palea Kameni, on the western coast of Santorini, and the island of Thirasia. The findings indicate that, in addition to the east-west horizontal displacements observed in different parts of the island, there were also vertical displacements on the island's surface, including both uplift and subsidence.

The long-term InSAR assessments applied in this study provide important geophysical indicators of the existence of volcanic activity-induced unrest in the region, whether it increases or decreases over time or whether it has begun to end. Even if these results are not signs of intense seismic activity or are evaluated together with earthquake data, it is possible to reveal volcanic-induced crustal deformations.

In future studies, modelling approaches based on longer InSAR time series and/or integrated with complementary observation techniques (e.g., GNSS, seismic data) may provide a more comprehensive understanding of the magmatic and tectonic mechanisms that could trigger such deformations.

Acknowledgements. We would like to acknowledge the Alaska Satellite Facility (ASF) for providing the Sentinel-1 radar data used in this study. Additionally, we express our gratitude to the European Space Agency (ESA) for their continuous support of the Copernicus program, which made the Sentinel-1 radar data publicly available. Some of figures in this paper were plotted using Generic Mapping Tools v6 (Wessel, 2019).

Funding. This research received no specific grant from any funding agency in the public, commercial, or not-for-profit sectors.

References

Aiuppa, A., D. Tamburello, R. Di Napoli, C. Cardellini et al. (2013). First observations of the fumarolic gas output from a restless caldera: Implications for the current period of unrest (2005-2013) at Campi Flegrei, Geochem. Geophys. Geosyst, 14, 4153-4169, doi:10.1002/ggge.20261.

Antoniou, V., F. L. Bonali, P. Nomikou, A. Tibaldi et al. (2020). Integrating virtual reality and GIS tools for geological mapping, data collection and analysis: an example from the Metaxa Mine, Santorini (Greece), Applied Sci., 10, 23, 8317, doi:10.3390/app10238317.

Arikan, M., A. Hooper and R. Hanssen (2010). Radar time series analysis over West Anatolia. In: Lacoste Francis H (editor). Fringe 2009 Proceedings, ESA SP 677. Noordwijk, Netherlands: ESA, 1-6.

Briole, P., A. Ganas, A. Serpetsidaki, F. Beauducel et al. (2025). Volcano-tectonic interaction at Santorini. The crisis of February 2025. Constraints from geodesy, Geophys. J. Int., 242, 3, ggaf262, doi:10.1093/gji/ggaf262.

Browning, J., K. Drymon and A. Gudmundsson (2015). Forecasting magma-chamber rupture at Santorini volcano, Greece Sci. Rep., 5, 15785, doi:10.1038/srep15785.

Chen, C. W. and H. A. Zebker (2001). Two-dimensional phase unwrapping with use of statistical models for cost functions in nonlinear optimization, J. Optical Soc. Am. A, 18, 2, 338-351, doi:10.1364/JOSAA.18.000338.

Del Gaudio, C., I. Aquino, G. P. Ricciardi, C. Ricco and R. Scandone (2010). Unrest episodes at Campi Flegrei: A reconstruction of vertical ground movements during 1905-2009. J. Volcanol. Geotherm. Res., 195, 48-56. doi:10.1016/j.jvolgeores.2010.05.014.

Dimitriadis, I., E. Karagianni, D. Panagiotopoulos, C. Papazachos et al. (2009). Seismicity and active tectonics at Coloumbo Reef (Aegean Sea, Greece): Monitoring an active volcano at Santorini Volcanic Center using a temporary seismic network, Tectonophysics, 465, 136-149, doi:10.1016/j.tecto.2008.11.005.

Druitt, T. H. (2014). New insights into the initiation and venting of the Bronze-Age eruption of Santorini (Greece), from component analysis. Bull. Volcanol. 76, 1-21. doi:10.1007/s00445-014-0794-x.

Druitt, T. H., D. M. Pyle and T. A. Mather (2019). Santorini volcano and its plumbing system. Elements:An International Magazine of Mineralogy, Geochemistry, and Petrology, 15(3), 177-184. doi:10.1144/GSL.MEM.1999.019.01.12.

Druitt, T. H., L. Edwards, R. M. Mellors, D. M. Pyle et al. (1999). Santorini Volcano. Geol. Soc. Mem. 19, 165. doi:10.2138/gselements.15.3.177.

Drymoni, K., J. Browning and A. Gudmundsson (2022). Spatial and temporal volcanotectonic evolution of Santorini volcano, Greece, Bull. Volcanol., 84, 6, 60, doi:10.1007/s00445-022-01566-4.

Feuillet, N. (2013). The 2011-2012 unrest at Santorini rift: stress interaction between active faulting and volcanism. Geophys. Res. Lett., 40, 3532-3537, doi:10.1007/s00445-022-01566-4.

Foumelis, M., E. Trasatti, E. Papageorgiou, S. Stramondo and I. Parcharidis (2013). Monitoring Santorini volcano (Greece) breathing from space, Geophys. J. Int., 193, 161-170, doi:10.1093/gji/ggs135.

Friedrich, W. L., B. Kromer, M. Friedrich, J. Heinemeier et al. (2006). Santorini eruption radiocarbon dated to 1627-1600 B.C. Science, 312, 548, doi:10.1126/science.11250.

Fuhrmann, T. and M. C. Garthwaite (2019). Resolving three-dimensional surface motion with InSAR: Constraints from multi-geometry data fusion, Remote Sensing, 11, 3, 241, doi:10.3390/rs11030241.

Gül, Y. and B. Poyraz (2024). Determination of long-term deformation behaviours with InSAR data at a dump site of an open-pit coal mine in Turkey, Adv. Space Res., 73, 3, 1667-1681, doi:10.1016/j.asr.2023.10.052.

Gül, Y., K. Ö. Hastaoğlu and F. Poyraz (2025). A new methodology for determining the long-term behavior of earth surface deformations from InSAR results, Adv. Space Res., 75, 4, 3521-3540, doi:10.1016/j.asr.2024.12.035.

Hanssen, R. F. (2001). Radar interferometry: data interpretation and error analysis, 2. Springer Science & Business Media.

Hastaoglu, K. (2016). Comparing the results of psınsar and GNSS on slow motion landslides, Koyulhisar, Turkey, Geomatics, Nat. Hazards Risk 7, 786-803, doi:10.1080/19475705.2014.978822.

Heath, B. A., E. E. E. Hooft, D. R. Toomey, C. B. Papazachos et al. (2019). Tectonism and its relation to magmatism around Santorini volcano from upper crustal P-wave velocity, J. Geophys. Res. 124, doi:10.1029/2019JB017699.

Hooft, E. E., P. Nomikou, D. R. Toomey, D. Lampridou et al. (2017). Backarc tectonism, volcanism, and mass wasting shape seafloor morphology in the Santorini-Christiana-Amorgos region of the Hellenic Volcanic Arc, Tectonophysics, 712-713, doi:10.1016/j.tecto.2017.06.005.

Hooper, A., P. Segall and H. Zebker (2007). Persistent scatterer interferometric synthetic aperture radar for crustal deformation analysis, with application to Volcán Alcedo, Galápagos, J. Geophys. Res.: Solid Earth, 112, B7, doi:10.1029/2006JB004763.

Hooper, A., D. Bekaert, E. Hussain and K. Spaans (2018). StaMPS/MTI Manual Version 4.1b. Delft Institute of Earth Observation and Space Systems Delft University of Technology, Kluyverweg.

Karátson, D., R. Gertisser, T. Telbisz, V. Vereb, et al. (2018). Towards reconstruction of the lost Late Bronze Age intra-caldera island of Santorini, Greece, Sci. Rep., 8, 7026, doi:10.1038/s41598-018-25301-2.

Kennedy, B. (2024). Underestimated volcanic hazard of Santorini, Nature Geosci., 17, 4, 278-279, doi:10.1038/s41561-024-01395-4.

Lagios, E., V. Sakkas, F. Novali, F. Belloti, et al. (2013). SqueeSAR™ and GPS ground deformation monitoring of Santorini Volcano (1992-2012): tectonic implications, Tectonophysics, 594, 38-59, doi:10.1016/j.tecto.2013.03.012.

Mountrakis, D., S. Pavlides, A. Chatzipetros, S. Meletlidis et al. (1998). Active deformation of Santorini. In: Proceedings of the 2nd Workshop on European Laboratory Volcanoes, Santorini, R. Casale, M. Fytikas, G. Sigvaldasson, G. Vougioukalakis, Eds., 13-22.

Newman, A. V., S. Stiros, L. Feng, P. Psimoulis et al. (2012). Recent geodetic unrest at Santorini Caldera, Greece, Geophys. Res. Lett., 39, doi:10.1029/2012GL051286.

Nomikou, P., C. Hübscher, M. Ruhnau and K. Bejelou (2016). Tectono-stratigraphic evolution through successive extensional events of the Anydros Basin, hosting Kolumbo volcanic field at the Aegean, Tectonophysics, 671, 202-217, doi:10.1016/j.tecto.2016.01.021.

Papadimitriou, P., V. Kapetanidis, A. Karakonstantis, G. Kaviris et al. (2015). The Santorini Volcanic Complex: a detailed multi-parameter seismological approach with emphasis on the 2011-2012 unrest period, J. Geodyn., 85, 32-57, doi:10.1016/j.jog.2014.12.004.

Papageorgiou, E., M. Foumelis, E. Trasatti, G. Ventura et al. (2019). Multi-sensor SAR geodetic imaging and modelling of Santorini volcano post-unrest response, Remote Sensing, 11, 3, 259, doi:10.3390/rs11030259.

Papageorgiou, E., M. Foumelis and I. Parcharidis (2012). SAR interferometric analysis of ground deformation at Santorini volcano (Greece), paper presented at the Fringe 2011 workshop, ESA, Frascati, Italy.

Papazachos, C., M. Foumelis, S. Bitharis, C. Pikridas et al. (2025). The Santorini 2024-2025 volcano-tectonic sequence: Constraining the initial phase of the intra-caldera unrest, Geophys. Res. Lett., 52, 13, e2025GL115856, doi:10.1029/2025GL115856.

Papoutsis, I., X. Papanikolaou, M. Floyd, K. H. Ji et al. (2013). Mapping inflation at Santorini volcano, Greece, using GPS and InSAR, Geophys. Res. Lett., 40, 2, 267-272, doi:10.1029/2012GL054137.

Parks, M. M., J. Biggs, P. England, T. A. Mather et al. (2012). Evolution of Santorini Volcano dominated by episodic and rapid fluxes of melt from depth, Nat. Geosci., 5, 10, 749-754, doi:10.1038/ngeo1562.

Pyle, D. M. (1997). The global impact of the minoan eruption of Santorini, Greece, Environ. Geol., 30, 59-61, doi:10.1007/s002540050132.

Sandwell, D., R. Mellors, X. Tong, M. Wei and P. Wessel (2011). Open radar interferometry software for mapping surface Deformation, Eos, Trans. Am. Geophys. Union, 92, 28, 234, doi:10.1029/ 2011eo280002.

Sandwell, D., R. Mellors, X. Tong, X. Xu et al. (2016). GMTSAR: An InSAR processing system based on generic mapping tools (second edition). In Scripps Institution of Oceanography Technical Report, doi:10.2172/1090004.

Stiros, S. C., P. Psimoulis, G. Vougioukalakis and M. Fytikas (2010). Geodetic evidence and modeling of a slow, small-scale inflation episode in the Thera (Santorini) volcano caldera, Aegean Sea, Tectonophysics, 494, 180- 190, doi:10.1016/j.tecto.2010.09.015.

Tekin, O. (2016). Eski Yunan ve Roma tarihine giriş. İletişim Yayınları, 349, İletişim Yayınları, Turkish version.

Wessel, P., J. F. Luis, L. A. Uieda, R. Scharroo, et al. (2019). The generic mapping tools version 6, Geochem., Geophys., Geosys., 20, 11, 5556-5564, doi:10.1029/2019GC008515.

Wicks, C. W., W. Thatcher, D. Dzurisin and J. Svarc (2006). Uplift, thermal unrest and magma intrusion at Yellowstone, doi:10.1038/nature04507.

***CORRESPONDING AUTHOR: Bekir POYRAZ**,
Department of Physics, Faculty of Science, Sivas Cumhuriyet University, Sivas, Türkiye
e-mail: bpoyraz@cumhuriyet.edu.tr